

A quantitative comparison of rates of phagocytosis and digestion of apoptotic cells by macrophages from normal (BALB/c) and diabetes-prone (NOD) mice

Athanasius F. M. Marée<sup>\*1</sup>, Mitsuhiro Komba<sup>\*2</sup>,  
Diane T. Finegood<sup>2</sup> and Leah Edelstein-Keshet<sup>3</sup>

<sup>1</sup>*Theoretical Biology/Bioinformatics,*

*Utrecht University, Utrecht, the Netherlands*

<sup>2</sup>*Diabetes Research Laboratory, School of Kinesiology,*

*Simon Fraser University, Burnaby, B.C., Canada*

<sup>3</sup>*Department of Mathematics and Institute of Applied Mathematics,*

*University of British Columbia, Vancouver, B.C., Canada*

*\*Both authors have contributed equally*

14th October 2007

**Running head:**

Phagocytosis and digestion by NOD mice macrophages

**Corresponding author:**

Leah Edelstein-Keshet

Mathematical Department

University of British Columbia

Vancouver, BC

V6T 1Z2, Canada

Phone 604-822-5889

Fax 604-822-6074

Email: keshet@math.ubc.ca

### Abstract

Macrophages play an important role in clearing apoptotic debris from tissue. Defective or reduced clearance, seen, for instance in non-obese diabetic (NOD) mice has been correlated with initiation of autoimmune (type 1) diabetes (T1D) (O'Brien et al., 2002b). To validate such a link, it is essential to quantify the reduced clearance (for example, by comparison to BALB/C control mice), and to determine which elements of that clearance are impaired. Recently, we fit data for the time course of *in vitro* macrophage feeding experiments to basic models of macrophage clearance dynamics, thus quantifying kinetics of uptake and digestion of apoptotic cells in both mouse strains (Marée et al., 2005). In the cycle of modeling and experimental investigation, we identified the importance of (1) measuring short, intermediate, and long-time data (to increase the accuracy of parameter fits), and (2) designing experiments with distinct observable regimes, including engulfment-only and digestion-only phases. Here we report on new results from experiments so designed. In comparing macrophages from the two strains, we find that NOD macrophage engulfment of apoptotic cells is 5.5 times slower than BALB/C controls. Significantly, our new data demonstrates that digestion is at least 2 times slower in NOD, in contrast with previous conclusions. Moreover, new data enables us to detect an acceleration in engulfment (after the first engulfment) in *both* strains, but much smaller in NOD macrophages.

**Keywords:**

NOD mice

autoimmune diabetes

macrophage phagocytosis

engulfment rate

digestion rate

# 1 Introduction

A variety of innate and adaptive immune system components are implicated in the destruction of  $\beta$ -cells in the pancreatic islets of Langerhans, causing autoimmune diabetes (type 1, T1D). Self-reactive T-cells are known to be the main effectors of  $\beta$ -cell killing (Höglund et al., 1999; Devendra et al., 2004). However, controversy exists as to the events that initiate the activation of  $\beta$ -cell-specific T-cells (Delovitch and Singh, 1997; O’Brien et al., 2002b). Macrophages are among the earliest cells to infiltrate the islets. In the non obese diabetic (NOD) mouse, a common animal model for T1D, this infiltration occurs as early as two weeks of age, and coincides with a normal wave of apoptosis of  $\beta$ -cells (Trudeau et al., 2000). This is followed by infiltration of dendritic cells, CD4<sup>+</sup> and CD8<sup>+</sup> T-cells at 6-10 weeks (Dahlén et al., 1998). Female NOD mice become diabetic by 12-15 weeks (Höglund et al., 1999) when 95% of their  $\beta$ -cells have been destroyed (Luppi and Trucco, 1999).

Relative to BALB/c (controls), macrophages of NOD mice are identifiably different (Shimada et al., 1994; Georgiou et al., 1995), exhibiting abnormal cytokine secretion (Alleva et al., 2000), reduced activation of other immune cells (Gordon, 1998; Jun et al., 1999), and reduced phagocytosis (O’Brien et al., 2002b). Based on these observations, it has been suggested that defective macrophage clearance of the neonatal wave of  $\beta$ -cell apoptosis leads to self-presentation and, subsequently, to T-cell activation (Trudeau et al., 2000; Mathis et al., 2001). In earlier mathematical models it has been shown that reduced macrophage clearance could be a major factor in T1D initiation (Freiesleben De Blasio et al., 1999; Marée et al., 2006). These observations have motivated an ongoing comparative study of macrophage behavior in NOD versus BALB/c mice.

We recently showed that inter-strain differences can be inferred by fitting time course data of *in vitro* macrophage feeding experiments to mathematical models of macrophage dynamics (Marée et al., 2005). Our previous study demonstrated the feasibility of determining multiple kinetic parameters from such data. Moreover, it identified the importance of measuring data on multiple timescales and at different regimes: one of the improvements described here is inclusion of a “digestion only” regime, to directly measure the rate that macrophages process apoptotic bodies after engulfment. Our main goal in this paper is to report on results of these redesigned experiments, and to show how these facilitate more accurate determination of clearance kinetics, and hence, better inter-strain comparison.

Before comparing between strains, we ask basic general questions about macrophage clearance: (Q1) After the first engulfment, do subsequent engulfments take place at higher rate? If so, we refer to the acceleration in engulfment as an “activation” step<sup>1</sup>. (Q1a) If activation is observed, is that activation reversible or irreversible on the timescale of several hours? (Q2) Is there evidence for a maximal capacity of engulfed apoptotic bodies in a macrophage? (Q2a) If so, what is that maximal number? (Q3) Are the engulfed apoptotic

---

<sup>1</sup>Our term “activation” should not be confused with similar term applied to transition of macrophages to antigen presenting cells or other changes in response to inflammatory stimuli.

bodies digested simultaneously or does digestion saturate?

In (Q1a) we distinguish between the case that a macrophage reverts to a quiescent state (reversible activation) after fully digesting a meal, or remains in an elevated engulfment mode (irreversible activation) over the time-scale of a few hours. In (Q3) we distinguish between (a) digestion that can handle many apoptotic bodies in parallel, (b) a saturated digestion machinery that can only break down one body at a time, and (c) a machinery that saturates only at higher numbers of apoptotic bodies. (Note that we refer to apoptotic cells pre-engulfment, and to apoptotic bodies while still visible inside a macrophage.) By comparing the quality of fit of data to several model variants, we distinguish between competing models and answer (Q1-3). Having identified the optimal model (and hence the most likely macrophage dynamics), we assess differences between the control (BALB/c) and diabetes-prone (NOD) mice.

## 2 Materials and Methods

### 2.1 Animals

Five-week-old female BALB/c and NOD/Lt mice (purchased from Taconic, Germantown, NY) had free access to standard laboratory chow and water. Before collection of peritoneal cells, mice were killed by CO<sub>2</sub> asphyxiation. Animals were handled in accordance with the regulations of the Canadian Council on Animal Care and all experimental manipulations of the animals were approved by the Animal Care Committee at Simon Fraser University.

### 2.2 Isolation and culture of macrophages

Non-elicited macrophages were collected from mice by peritoneal lavage with cold complete medium (RPMI 1640; 100 units/mL penicillin, 100  $\mu$ g/mL streptomycin, and 10% vol/vol heat-inactivated fetal calf serum (FCS), all from Life Technologies, Burlington, Ontario, Canada). Macrophages from multiple mice of a given strain were pooled together and aliquots were seeded into eight-well chamber slides (Nalge Nunc, IL). Cells were incubated at 37°C/5% CO<sub>2</sub> for 2 hours, allowing macrophages to adhere and spread on the slides. Unbound cells were washed three times with phosphate-buffered saline (PBS), then cultured with apoptotic cells. The resulting number of adherent macrophages was approximately  $1 \cdot 10^5$  cells per well.

### 2.3 Induction of apoptosis

A suspension of thymocytes harvested from BALB/c mice was irradiated by exposure to 254 nm ultraviolet C light for 20 min, then cultured in serum-free complete medium for 2h at 37°C/5 % CO<sub>2</sub> to let apoptosis progress. FCS (10% vol/vol) was then added to the medium.

## 2.4 Phagocytosis and digestion assays

Apoptotic cells were cultured with macrophages at a ratio of 5:1 apoptotic cells-to-macrophages at 37°C/5% CO<sub>2</sub> for variable periods of time. A total of 6 wells were used for each strain of mice for each experiment. Each well was assigned a specific time point: 20 min, 1h, 2h, 3h, 4h, and 5 h. After 20 min, 1h and 2 h, cells from one well per strain of mouse were washed three times with PBS to remove apoptotic thymocytes that had not been phagocytosed. For the “engulfment” experiment, cells were then fixed in 10% neutral buffered formalin (Sigma, Oakville, Ontario, Canada), and stained with Mayer’s haematoxylin and eosin (H&E) (Sigma) for identification of apoptotic thymocytes and macrophages.

For the “digestion-only” phase, at the end of 2-hour coculture of macrophages and apoptotic cells, the remaining three wells per strain were washed with PBS to remove residual (unengulfed) apoptotic cells. Complete medium was then added to the wells, and adherent cells were further cultured for 1h, 2h, or 3h (for the time endpoints at 3h, 4h, and 5h, respectively, on Fig 2). At the end of a culture period, cells were washed, fixed, and stained as above. Cells were observed with light microscopy at 1000-fold magnification under oil immersion.

Phagocytosis was evaluated by counting and classifying approximately 1000 macrophages per well. Altogether, 60 wells (30 per strain) were analyzed, with a total of 58,646 macrophages. Each macrophage was assigned to a class ( $i = 0, 1, 2, \dots N$ ) according to the number,  $i$ , of internalized apoptotic bodies it contained. Generally, up to  $N = 7$  internalized apoptotic bodies could be observed, but sporadically even larger numbers, up to eleven were seen. Only apoptotic bodies clearly visible within the perimeter of the macrophage were counted. Results were initially expressed as the fraction of macrophages within a certain class in each well. These numbers were subsequently converted into macrophage densities (in units of cells/mL), by multiplying the fraction by the number of adherent macrophages per well ( $1 \cdot 10^5$ ) and dividing it by the well volume (0.5 mL).

## 2.5 Modeling techniques

Our modeling techniques are based on Marée et al. (2005). Definitions of all variables and parameters are given in Tables 1 and 2 and a full composite of the models is shown in Figure 1. These include phagocytosis with and without an activation step (which is either reversible or irreversible), three variants of digestion (parallel, serial, and saturating) and two distinct maximal number of engulfed bodies per macrophage ( $N=7$  or 12). In each case,  $M_i(t)$  represents the number of macrophages that contain  $i$  visible apoptotic bodies at time  $t$  (hrs), with  $i= 0, 1, 2$ , etc. up to  $N$ , and  $A$  is the remaining number of unengulfed apoptotic cells. Macrophages “transit” between classes by engulfing apoptotic cells (arrows pointing right in Figure 1), using up  $A$ , or by digesting an internalized cell (arrows to left). On the time scale of the experiment (5h), the macrophage population is approximately constant ( $2 \cdot 10^5$  cells/mL).

We simplify the macrophage clearance (targeting, binding, engulfing and digesting apoptotic or necrotic cells) as essentially two processes, each with its own inherent timescale, engulfment (represented by parameter  $k_e$  [mL cell<sup>-1</sup> h<sup>-1</sup>]), and digestion (represented by parameter  $k_d$  [h<sup>-1</sup>]). Experimental evidence (Erwig et al., 1999; Licht et al., 2001; O’Brien et al., 2002b) suggests that, after the first engulfment, subsequent engulfment are either faster (Licht et al., 2001; O’Brien et al., 2002b), or slower (Erwig et al., 1999) than the initial rate. To allow for either case, we use  $k_a$  [mL cell<sup>-1</sup> h<sup>-1</sup>] to represent the initial engulfment rate and  $k_e$  for the later rates. (Because we find that  $k_a < k_e$ , we later refer to  $k_a$  as the “activation rate” and the basal engulfment state before activation as the “rest state”.) We considered two cases: (i) macrophages stay activated on the experimental time-scale vs (ii) return to rest state after fully digesting a meal. (See, e.g., (Licht et al., 2001) who observe higher engulfment rates even after 20 h.)

We considered several possible maximal capacities of apoptotic bodies per macrophage,  $N$ . In one case,  $N$  was set to the maximum observed experimentally; we also tested a much larger value, and a third case where such a limit does not exist. As details of the digestion process are not known, we considered the following possibilities: (1) a saturating Michaelian rate of the form  $k_d i / (c + i)$ , where  $i$  is the load (i.e., number of apoptotic bodies to be digested), and  $c$  the load at half-saturation. (2) a linear regime, with rate  $(k_d/c)i = k'_d i$  (which approximates regime (1) if saturation occurs only at a very high load. This is termed “parallel digestion” since the time to digest any load  $i$  is the same. (3) Serial digestion, i.e. the opposite regime where the process is fully saturated, and the digestion rate is  $k_d$ .

To avoid combinatorial proliferation of possible models, we here discuss a subset of models chosen to explore the main features of interest (Fig. 1).

**Basic Model:** The engulfment rates are all identical ( $k_{e0} = k_e$ ), and digestion is serial with identical constant rates ( $k_{d1} = k_{d2} = k_{d3} = k_d$ ). See Fig. 1(a).

**Variants I, II: Reversible/Irreversible activation:** The first and subsequent engulfments occur at distinct rates, ( $k_{e0} = k_a \neq k_e$ ). In I, we identify the first step as a reversible activation step, which means that digesting the last apoptotic body brings the macrophage back to the rest state (Fig. 1(a)). In II we included a separate class,  $M_{0a}$ , of activated macrophages without apoptotic bodies. Only the resting macrophages, denoted  $M_{0r}$  in this variant, have a distinct engulfment rate  $k_{e0} = k_a \neq k_e$  (Fig. 1(b)). The classes  $M_{0a}, M_{0r}$  cannot be distinguished experimentally, but can be determined by fitting the data to the model.

**Variants III, IV: Parallel/Serial digestion:** In III, we modified Variant II by assuming parallel digestion, i.e.  $k_{d1} = k'_d, k_{d2} = 2k'_d, k_{d3} = 3k'_d, k_{di} = ik'_d$ . In IV, we assumed Michaelian digestion rates,  $k_{d1} = k_d/(c + 1), k_{d2} = 2k_d/(c + 2), k_{d3} = 3k_d/(c + 3), k_{di} = k_d i / (c + i)$  where  $i$  is the number of apoptotic bodies to digest and  $c$  is the number at which digestion is at half of its maximal rate.

## 2.6 Parameter fitting and Model Comparison

As in Marée et al. (2005), we fit parameters in two ways, first by using simple features of the data and second, by full fitting using the freeware biochemical simulator program Gepasi and its Levenberg-Marquardt optimization routine (Mendes, 1993, 1997; Mendes and Kell, 1998).

Because cells have to be fixed before counting, the closest we can get to a true time-series is to run experiments concurrently, using a single aliquot of macrophages for all wells. We call such a time series “a single replicate”. In a concurrent fit, we fit to all data points of all replicates simultaneously, though they are obtained from different aliquots of macrophages. Here, a confidence interval for parameter values can be calculated, based on the drop in the goodness-of-fit when each individual parameter is changed. (Alternately, fitting each replicate separately preserves the distinction between aliquots.) With replicate fitting, one can calculate the standard deviation in the default way, because the outcome of the fittings can be considered to be five independent measurements of the same kinetic constant. By comparing the quality-of-fit between concurrent and replicate fitting, we can also determine if there are significant differences between replicates (which would warrant critical evaluation of the experimental setup). A full discussion of the advantages and disadvantages of each method is provided in Marée et al. (2005).

To select the model that best fits the observed data, we used the Akaike’s Information Criterion (AIC) (Akaike, 1973; Motulsky and Christopoulos, 2003). The criterion selects the model that has greatest accuracy with fewest free parameters<sup>2</sup>. (See Appendix and fuller discussion in Marée et al. (2005).) The Akaike weights,  $w_i$  (Table 5), represent the relative probability of each candidate out of a set of models being the best representation of the dynamics underlying the data. We also used this criterion to compare concurrent vs. replicate data fits.

## 3 Results

We describe parameter values from ballpark estimates and from full data fits. Our procedure is explained below, and the results are summarized in Tables 3 and 4. The last column in these tables is the predicted fold difference in the parameter values between NOD and BALB/c mice, and the 95% likelihood interval, calculated using the default Student t-test to compare two samples with different standard deviations. An asterisk indicates  $P < 0.05$ .

---

<sup>2</sup>By introducing more free parameters, it becomes easier to fit the data more closely, and therefore, AIC penalizes each additional parameter.

### 3.1 Ballpark parameter estimates

Our models use features of experimentally observed dynamics of macrophage classes (Table 1) to compute rough estimates of parameters for individual macrophage function (Table 3). The relevant formulae are based on simple features of the data such as slopes ([s0, s1, s2]), ratios ([r1]), and other descriptors ([p1], [i1]) as summarized in Table 2, and cited by tags in square brackets here. (For full derivations, see Marée et al. (2005).) For accurate parameter fits, observations are needed at early ( $t_1 = 20$  min), and intermediate ( $t_Q = 1, 2$  h) time points, as well as in the digestion phase ( $t_d=2, 3, 4, 5$  h, after washing out remaining apoptotic cells). The quality of the estimates improves if  $A$  is also measured at each time point (not possible in our experiments).

#### Early time points

In the beginning of the experiment, all macrophages are in class 0 ( $M_0 = M$ ). The dominant process, engulfment, is then related to the rate of decrease of  $M_0$  and/or rate of increase of  $M_1$ , i.e. to the initial slope of the data curve. An approximation of this derivative using a finite difference of data values (at discrete times, e.g., Eq. (3)) is reasonable provided time points are close together. This early time data is thus used to estimate the engulfment rates ( $k_e$  in the Basic Model ([e1,e2]), and  $k_a$  in variants I and II, [a1]). In the basic model, all subsequent engulfments are identical. In activation-variant models, the rates of (subsequent) engulfments can be obtained by rates of change of higher classes at early time points ([e3]). Time points too far apart underestimate these parameters.

#### Distribution of macrophage classes and parameter ratio

After about 1 h of feeding, the number of apoptotic cells and ability of macrophages to engulf and digest equilibrate. This approximate equilibrium is termed a quasi-steady state (QSS). At this time ( $t = t_Q$ ), ratios of the sizes of successive classes are roughly constant ([r1]), that is  $M_1/M_0 \approx M_2/M_1 \equiv R = \text{constant}$ . Further, in the Basic Model, it can be shown that this ratio is related to a ratio of model parameters:

$$R = \text{Ratio of number of macrophages in successive classes} = \frac{k_e A}{k_d}. \quad (1)$$

If  $A$  is observed experimentally, this ratio can be used to calculate  $k_d$  based on the previously obtained  $k_e$  value ([d1]).

#### Estimates for the digestion rate

Studies of phagocytosis often cite the *percent phagocytosis*  $\Phi$  (the percent of macrophages that have engulfed one or more apoptotic cells), and the *phagocytic index*  $I_\Phi$  (the number of



visible apoptotic bodies per 100 macrophages) (O’Brien et al., 2002a,b). These indices ([p1, i1]) are helpful in obtaining an estimate of the digestion rate, and they are also related to the ratio  $R$  ([r3, r4]).

In the digestion phase, apoptotic cells have been washed out ( $A = 0$ ), and no further engulfments occur, so each macrophage gradually digests its meal and “transits” to a lower class. The number of macrophages in a certain class could still increase, due to a large influx of macrophages from a higher class, but the total number of apoptotic bodies within all macrophages should continuously decrease. In the case of parallel digestion, the decrease in total number of apoptotic bodies should be exponential. Thus, the phagocytic index,  $I_\Phi$  (which is the relative total number of apoptotic bodies), should also decrease exponentially (Appendix Eq. (4)). Hence, it follows that

$$k'_d = \frac{1}{T} \ln \left( \frac{\tilde{I}_\Phi}{I_\Phi} \right). \quad (2)$$

Here  $\ln()$  is the natural logarithm,  $\tilde{I}_\Phi$  is the phagocytic index at the start of the digestion phase ( $t = t_{d0} = 2$  h), and  $T$  is elapsed time ( $T = t - t_{d0}$ ). (See formula [d4].)

A number of other formulae ([d2, d3, e4, e5]) link various ratios and parameters. All have been derived for our specific set of models, but these can be generalized to other situations.

### 3.2 Model comparison by full data fits

Because the above estimates are fairly rough, for model comparison we use full data fits. We compare all model variants (and concurrent vs. replicate data fits) in Table 5 to select the best model. Rows 1-12 compare models for BALB/c data, and rows 13-24 for NOD data. The last 12 rows compare digestion variant models using only the digestion data.

**Macrophage activation:** We find that models with an activation step are more likely than the Basic Model, and that consecutive engulfments are indeed faster than the initial engulfment. ( $k_e$  is significantly different and always higher than  $k_a$ , contrary to reports in Erwig et al. (1999)). Reversible and irreversible activation are found to be equally likely (Variant I, II, Table 5). The fact that activation is an important feature of the behavior in both strains is a new result that differs from our previous conclusions.

**Macrophage capacity:** In Variant II, comparing  $N = 7$  to  $N = 12$  results in no difference in fit. If there were an underlying maximum capacity, the model with  $N = 12$  that predicts higher levels of apoptotic bodies would have a lower goodness-of-fit, and be less likely. Since the same dynamics (and therefore the same likelihood) are predicted for  $N = 12$  and higher  $N$ , a phagocytosis ceiling did not play a role in our experiments. (If such a ceiling exists, a much larger meal of apoptotic cells would be needed to detect it; this would fill higher  $M_i$

classes.) Our data indicates that the observed maximum number of apoptotic bodies per macrophage, 7 is not due to limitations on further engulfment.

**Serial, parallel or saturating digestion:** Serial digestion is most probable for both strains in each case. Although the SSE is lower for the saturating model (IV), the improvement of fit is too small to justify an extra parameter, so serial digestion most parsimoniously explains the data. However, for NOD macrophages, parallel and saturating digestion (Variants III and IV) still have significant probability of best describing the data. Because NOD mice have strongly reduced phagocytic capabilities, only a small fraction of their macrophages are in higher classes. Thus, it becomes harder to compare digestion rates for different classes, as needed to discriminate between the digestion model variants. Altogether, our model comparisons indicate that digestion is best described as a serial process in both mouse strains.

**Replicate or concurrent fitting:** The likelihood of the replicate models is essentially zero. That is, we find no indication for variation in experimental set-up or performance between replicates. There is effectively no replicate-to-replicate variation in the kinetic constants. This observation allows us to extrapolate from the outcome of this study (i.e. the estimated parameter values) to more general quantitative questions about the dynamics underlying the development of diabetes in NOD mice (see Marée et al., 2006).

### 3.3 Parameter values obtained

The results of full fitting of models to concurrent data using the optimization feature of the software Gepasi are shown in Table 4. Clear differences emerge between the parameters for control (BALB/c) versus diabetes-prone (NOD) mice, revealing details not apparent from the ballpark estimates of Table 3. As discussed in model comparisons, the parameter values given by model variants I and II should best estimate macrophage clearance dynamics, with variant II ( $N = 7$ ) having the highest likelihood for both strains. We compare across models and strains, below. Values are given for variant II ( $N = 7$ ) unless otherwise indicated.

**Engulfment rates:** The initial engulfment rates  $k_a$  are  $2.59 \pm 0.03$  times greater for BALB/c than for NOD macrophages, and subsequent engulfment rates,  $k_e$ , differ more dramatically, (by  $5.54 \pm 0.12$ , see Table 4). Model variants I and II ( $N = 12$ ) give highly comparable parameter estimates. This confirms that NOD macrophages are strongly impaired in engulfment. The rough estimates for  $k_a$  (Variant I, Table 3) are both qualitatively and quantitatively close to the full data fit values. Qualitatively, the ratios of BALB/c to NOD  $k_e$  values are similar for both fitting methods, but absolute levels are lower in ballpark estimates than in full data fits. The engulfment rate estimated by the full fit of the Basic Model is between the initial and subsequent rate; the ballpark estimate simply gives

the initial rate. In summary, the ballpark estimates give a reasonable representation of the engulfment dynamics.

**Activation:** For BALB/c macrophages, Table 4 reveals a clear difference between the rate of engulfment of the first apoptotic cell  $k_{eo} = k_a = 5.4 \cdot 10^{-7} \text{mL cell}^{-1} \text{h}^{-1}$ , and the subsequent, much faster engulfment rate  $k_e = 23.6 \cdot 10^{-7} \text{mL cell}^{-1} \text{h}^{-1}$  (more than five times higher). There is also a small but significant activation step in NOD, from  $k_a = 2.1 \cdot 10^{-7} \text{mL cell}^{-1} \text{h}^{-1}$ , to  $k_{eo} = k_a = 4.3 \cdot 10^{-7} \text{mL cell}^{-1} \text{h}^{-1}$ . In the ballpark estimates, increases in the engulfment rates are strongly underestimated, and hardly reveal any activation in the NOD case. (Full data fitting becomes essential for such fine detail). Importantly, in contrast with Marée et al. (2005), the fact that NOD macrophages also undergo activation could only be observed using both the improved dataset and full parameter fitting.

**Digestion rates:** The rate of digestion of the internalized apoptotic cells are  $2.41 \pm 0.05$  as large in BALB/c as in NOD. (For model variant I, a smaller fold-difference ( $1.97 \pm 0.05$ ) is observed.) This means that digestion is impaired in NOD macrophages, but not as dramatically as engulfment. The number of apoptotic bodies at half-saturation (variant IV) is  $c \approx 1$  for NOD and lower for BALB/c: in both strains, a single apoptotic body nearly saturates digestion. This explains why the experimental data is much better described by serial digestion (the immediate saturation extreme) than by parallel digestion (the no saturation extreme). The ballpark digestion rates are quite similar, but clearly overestimated. Only the parallel digestion estimate (Variant III) based on the digestion-only phase, is similar to the full data fit. Together, this shows that for good ballpark estimates of  $k_d$  it is essential to include a digestion phase in the experiments (unless the number of remaining apoptotic cells,  $A$ , is measured during the experiment). Otherwise, the accuracy of  $k_d$  is quite limited, as a consequence of being estimated indirectly. The more accurate data for the digestion phase and full data fits revealed a previously undetected inter-strain difference.

### 3.4 Displayed dynamics

Figures 2-3 show the dynamics of the macrophage engulfment models fit to data. We show the most likely model (variant II,  $N = 7$ ), and compare it with the basic model (without activation) and variant IV (which gave the best but not the most parsimonious fit). The performance of BALB/c macrophages (left column) is visibly more vigorous than NOD (right column). A comparison of left panels shows that a model with an activation step fits BALB/c data significantly better than the Basic Model (compare black curves in each case). In the NOD fits, the disparity between models with and without activation is not as strong, but the Basic Model is also not as accurate as the models with an activation step (compare green curves). These results contrast with Marée et al. (2005), where we found no significant improvement in the likelihood of a model with activation for NOD macrophages. Visually,

no improvement of the fit can be observed for variant IV, so the usage of an extra parameter is not justified.

Figure 3 shows the phagocytosis index ( $I_\Phi$ ) and percent phagocytosis ( $\Phi$ ) time courses. These curves were not fit separately, and give an independent indication of relative performance of models against data. Squares and triangles are  $\Phi, I_\Phi$  values computed from each data point, and curves are computed from model predictions using the best fit parameters in Table 4. The top left panel confirms that the Basic Model does not account for the behavior of BALB/c macrophages, since the black curve representing  $I_\Phi$  is significantly lower than the data points. In NOD mice (right panels), the distinction is not as great.

We computed the remaining unengulfed apoptotic cells,  $A$ , that could not be directly observed experimentally (simulations not shown). We found a huge difference systematically predicted between BALB/c and NOD mice: in two hours, BALB/c macrophages clear 30% of the available apoptotic cells, compared with less than 10% for NOD mice.

## 4 Discussion

### Major conclusions and insights

The results in this paper help to more accurately elucidate quantitative differences between macrophages in NOD mice prone to a form of autoimmune (type 1) diabetes compared to control (BALB/c) mice. In agreement with previous work, we found that NOD mouse macrophages have a slow rate of engulfment of apoptotic cells compared to controls (O’Brien et al., 2002b; Marée et al., 2005). (Even after activation, in NOD’s engulfment rate is less than one fifth of controls.) Like Marée et al. (2005), but unlike older papers, we here quantified biological parameters that represent the actual rates of phagocytosis of apoptotic cells, and the rate of digestion of those cells once they are engulfed. In contrast with Marée et al. (2005), a new major conclusion, based on the new refined experiments is that activation is an important feature in both strains. An extension of Marée et al. (2005) and a second major conclusion is that digestion is serial (rather than saturating or parallel).

Our models informed experimental design twice (see Table 6 for an overview): (A) models indicated that early time data is essential for accurate parameter estimates because intermediate time data only reveal quasi-steady state ratios (such as  $R$ ), rather than individual parameter values. Thus, inaccurate engulfment rates engender poor estimates for digestion rates, since these parameters are linked. Furthermore, without early data, the distinction between models with and without an activation step is blurred. (B) Even with early data (Marée et al., 2005) but without observing remaining apoptotic cells directly, a “ridge” in the parameter landscape hindered optimization of parameter fits. We then redesigned experiments to include early, middle, and late time behavior as well as a separate digestion phase; this led to proper estimation of the digestion rates, and hence, all linked parameters. A third major conclusion of this work is that, unless  $A$  can be observed over the course of the

experiment, it is important to obtain data from a digestion-only phase of the experiments.

The various ballpark estimates link population-level phenomena (distribution of macrophages into classes) to underlying cellular behavior (individual macrophage rates of activation, engulfment, and digestion of apoptotic cells). These estimates are less accurate than full fits, but reveals some interesting features. For example, the percent phagocytosis,  $\Phi$ , is simply proportional to the quantity we called  $R$ , which contains a ratio of engulfment and digestion rates. (The phagocytic index,  $I_\Phi$  is also related to  $R$ , but not as simply). This suggests that simple ratios of  $\Phi$  could be more easily interpreted than ratios of  $I_\Phi$  (see [r2] versus [r3] in Table 2) to compare values of  $k_e/k_d$  across strains.

From Tables 3 and 4, highly significant fold-differences between strains can be observed. (An asterisk in the last column indicates  $P < 0.05$ ). It is possible that the fitting method underestimates the standard deviation in the parameter values, since it does not take into account the possible covariance between parameters. (This could lead to less dramatic drops in quality-of-fit when parameters are varied concurrently.) However, even the rough estimates in Table 3 obtained from formulae in Table 2 demonstrate significant differences between NOD and BALB/c strains. These, and also comparisons of parameter estimates from different cohorts (data not shown) lead to much larger confidence intervals, but nevertheless, the fold-differences remain highly significant.

Assessing the relative merits of rough (Tables 3) and full (Table 4) parameter fits, we found that full fits using optimization software achieve more accurate results, as expected, but that the two sets of results are in the same order of magnitude. Furthermore, the ratios of rate constants for control and NOD mice are roughly the same. This implies that ballpark estimates would suffice to compare two conditions or strains, whereas full fits improve the absolute values of the parameters.

For model comparison, the Akaike criterion has wide applicability, wherever the details of underlying mechanisms are not known in advance. Using this technique, with the combined dataset from this experiment and from the first 2 h of the experiments reported in Marée et al. (2005), we found that the variants I and II (reversible and irreversible activation) provide the most probable candidates for both BALB/c and NOD. To properly distinguish between these two variants, one should perform experiments in which the macrophages are presented a second apoptotic meal after the first digestion phase. Similarly, to investigate whether there is truly a maximum number of apoptotic bodies that can be found within a single macrophage (as well as to determine its value), one should feed macrophages with a higher density of apoptotic cells than was used in the current experiments.

## Implications and connections with autoimmunity

A major difference between mouse strains is that in NOD macrophages, the engulfment rate of apoptotic cells is abnormally low by a factor between 2.6 and 5.5. A minor difference is in reduced degradation of apoptotic cells once they are engulfed. Here we mention some of

the implications of our results in the context of autoimmunity and pathogenesis of Type 1 diabetes (Trudeau et al., 2000; Mathis et al., 2001).

Aside from *in vitro* experiments, we have recently shown a systemic defect in NOD macrophages *in vivo* (in the peritoneum, the skin, and the thymus, O'Brien et al. (2006)). Challenging the NOD mouse with UV irradiation to the skin results in an increased apoptotic cell load (relative to control strains) and increased antibodies to DNA in circulation. Macrophage defects of a similar type have also been inferred in other autoimmune animal models, e.g., mice prone to lupus (Potter et al., 2003; Cohen et al., 2002). Mice that lack a membrane tyrosine-kinase (c-mer) have defective macrophage phagocytosis and are prone to a form of autoimmunity which resembles lupus (Cohen et al., 2002); a mutant protein in mice that masks phosphatidylserine on apoptotic cells inhibits the phagocytosis of those cells, which then leads to autoantibody production in the animals (Asano et al., 2004). All these experimental studies link autoimmunity and defective clearance of apoptotic cells.

A connection to human disease has also been made. Reduced clearance of apoptotic cells has been observed in human patients with systemic lupus erythematosus (SLE) (Herrmann et al., 1998). Gaipf et al. (2007) showed that apoptotic cells accumulate in germinal centers of the lymph nodes and in the skin of SLE patients after exposure to UV light. They showed that attraction signals for macrophages were lower in the sera of about one quarter of the patients, and suggested that defective clearance of dying cells could explain the accumulation of nuclear autoantigens in those patients. (See also Gaipf et al. (2006) for a recent review, but note the contrasting study by (Reefman et al., 2006) where clearance rates of apoptotic cells were not significantly different.)

There are a number of hypotheses about the causes underlying the link between phagocytic defects and autoimmunity. One suggestion is that residual apoptotic material undergoes secondary necrosis and results in inflammation due to release of endogenous chemical danger signals (Gallucci et al., 1999). Whether apoptotic cells also release such inflammatory signals is still controversial, but it has been shown recently that Jurkat cells release strong danger signals (high mobility group box 1 protein) to the extracellular environment 30 hours after induction of apoptosis with pharmacological agents such as staurosporine (Bell et al., 2006). While not verified experimentally, if secondary necrotic  $\beta$ -cells release such danger signals, this could induce maturation of dendritic cells that then prime naive autoreactive T cells. Furthermore, in some circumstances, inflammatory stimuli appear to reduce macrophage phagocytic ability, for example, in rat alveolar macrophages exposed to prolonged low levels of interferon- $\gamma$  (Camner et al., 2002); this could lead to a positive feedback loop, further decreasing clearance.

Macrophages are known to play a role in the digestion of DNA from apoptotic cells (McIlroy et al., 2000; Odaka and Mizuochi, 2002). Our new finding in this paper, that there are differences in this process (though to a lesser degree than differences in engulfment) between diabetes-prone and diabetes-resistant mice could also have implications in autoimmunity. It has been shown that mice whose macrophages lack DNase II in lysosomes exhibit an au-

toimmune phenotype, polyarthritis, similar to human rheumatoid arthritis. Kawane et al. (2006) showed that when macrophages cannot degrade DNA from apoptotic cells, they produce TNF- $\alpha$ , stimulating other cytokine production and culminating in chronic polyarthritis. Apoptotic cells (such as Jurkat cells) release DNA into their medium *in vitro* (Choi et al., 2004). DNA that escapes degradation, or is released from macrophages could cause immune response to self-tissues and initiate autoimmunity. This could be yet another mechanism linking defects in macrophage digestion to the pathogenesis of autoimmune diabetes.

Using an extension and revision of the Copenhagen model (Freiesleben De Blasio et al., 1999) with parameter values determined in Marée et al. (2005), and taking the inflammatory effect of necrotic  $\beta$ -cells into account, we have shown that inefficient clearance of apoptotic  $\beta$ -cells by macrophages can, by itself, give rise to prolonged chronic inflammation for NOD, but not BALB/c mouse parameters (Marée et al., 2006). This chronic inflammation could then set the stage for the development of T1D. In a later modeling study, Mahaffy and Edelstein-Keshet (2007), we showed that the difference in clearance rates of apoptotic debris (and thus, of putative auto-antigen peptides) between mouse strains can account for the fluctuating dynamics of CD8<sup>+</sup> T cells observed by Trudeau et al. (2003) in the pre-diabetic phase in NOD mice but not in controls. When clearance rates are normal, an immune stimulus that primes T cells gets resolved to a baseline state after a short time, and no autoimmunity occurs. A reduction of the clearance rate by a factor of 2 or more, as found here for NOD mice, could lead to cycles in the prevalence of auto-reactive T cells in our model, with eventual elevated levels of effector cells, autoimmunity, and death of  $\beta$ -cells.

In view of the above, our results have implications that go beyond simple quantification of phagocytosis. Indeed, such links suggest that macrophage clearance plays an important role in preventing autoimmunity, and that defects in that function could account for pathogenesis in T1D. Treating macrophage defects and enhancing the low engulfment rate of apoptotic material in diabetes-prone animals could be an additional strategy in retarding autoimmune diseases such as Type 1 diabetes.

## Grants

We gratefully acknowledge support by the Mathematics of Information Technology and Complex Systems (MITACS) and by the Juvenile Diabetes Research Foundation (JDRF). AFMM is supported by the Netherlands Organization for Scientific Research (NWO). LEK is also supported by the Natural Sciences and Engineering Research Council, NSERC (Canada). DF is also supported by the Canadian Institutes of Health Research.

## References

**Akaike H.** Information theory as an extension of the maximum likelihood principle. In: *Second International Symposium on Information Theory*, edited by Petrov BN, Csaki F,

Budapest: Akademiai Kiado, pp. 267–281, 1973.

**Alleva DG, Pavlovich RP, Grant C, Kaser SB, Beller DI.** Aberrant macrophage cytokine production is a conserved feature among autoimmune-prone mouse strains: elevated interleukin (IL)-12 and an imbalance in tumor necrosis factor- $\alpha$  and IL-10 define a unique cytokine profile in macrophages from young nonobese diabetic mice. *Diabetes* 49: 1106–1115, 2000.

**Asano K, Miwa M, Miwa K, Hanayama R, Nagase H, Nagata S, Tanaka M.** Masking of phosphatidylserine inhibits apoptotic cell engulfment and induces autoantibody production in mice. *J Exp Med* 200: 459–467, 2004.

**Bell CW, Jiang W, Reich CF, Pisetsky DS.** The extracellular release of HMGB1 during apoptotic cell death. *Am J Physiol Cell Physiol* 291: C1318–C1325, 2006.

**Camner P, Lundborg M, Låstbom L, Gerde P, Gross N, Jarstrand C.** Experimental and calculated parameters on particle phagocytosis by alveolar macrophages. *J Appl Physiol* 92: 2608–2616, 2002.

**Choi JJ, Reich CF, Pisetsky DS.** Release of DNA from dead and dying lymphocyte and monocyte cell lines in vitro. *Scand J Immunol* 60: 159–166, 2004.

**Cohen PL, Caricchio R, Abraham V, Camenisch TD, Jennette JC, Roubey RAS, Earp HS, Matsushima G, Reap EA.** Delayed apoptotic cell clearance and lupus-like autoimmunity in mice lacking the c-mer membrane tyrosine kinase. *J Exp Med* 196: 135–140, 2002.

**Dahlén E, Dawe K, Ohlsson L, Hedlund G.** Dendritic cells and macrophages are the first and major producers of TNF- $\alpha$  in pancreatic islets in the nonobese diabetic mouse. *J Immunol* 160: 3585–3593, 1998.

**Delovitch TL, Singh B.** The nonobese diabetic mouse as a model of autoimmune diabetes: immune dysregulation gets the NOD. *Immunity* 7: 727–738, 1997.

**Devendra D, Liu E, Eisenbarth GS.** Type 1 diabetes: recent developments. *BMJ* 328: 750–754, 2004.

**Erwig LP, Gordon S, Walsh GM, Rees AJ.** Previous uptake of apoptotic neutrophils or ligation of integrin receptors downmodulates the ability of macrophages to ingest apoptotic neutrophils. *Blood* 93: 1406–1412, 1999.

**Freiesleben De Blasio B, Bak P, Pociot F, Karlsten AE, Nerup J.** Onset of type 1 diabetes: a dynamical instability. *Diabetes* 48: 1677–1685, 1999.



- Gaipl US, Kuhn A, Sheriff A, Munoz LE, Franz S, Voll RE, Kalden JR, Herrmann M.** Clearance of apoptotic cells in human SLE. *Curr Dir Autoimmun* 9: 173–187, 2006.
- Gaipl US, Munoz LE, Grossmayer G, Lauber K, Franz S, Sarter K, Voll RE, Winkler T, Kuhn A, Kalden J, Kern P, Herrmann M.** Clearance deficiency and systemic lupus erythematosus (SLE). *J Autoimmun* 28: 114–121, 2007.
- Gallucci S, Lolkema M, Matzinger P.** Natural adjuvants: endogenous activators of dendritic cells. *Nat Med* 5: 1249–1255, 1999.
- Georgiou HM, Constantinou D, Mandel TE.** Prevention of autoimmunity in nonobese diabetic (NOD) mice by neonatal transfer of allogeneic thymic macrophages. *Autoimmunity* 21: 89–97, 1995.
- Gordon S.** The role of the macrophage in immune regulation. *Res Immunol* 149: 685–688, 1998.
- Herrmann M, Voll RE, Zoller OM, Hagenhofer M, Ponner BB, Kalden JR.** Impaired phagocytosis of apoptotic cell material by monocyte-derived macrophages from patients with systemic lupus erythematosus. *Arthritis Rheum* 41: 1241–1250, 1998.
- Höglund P, Mintern J, Waltzinger C, Heath, W. Benoist C, Mathis D.** Initiation of autoimmune diabetes by developmentally regulated presentation of islet cell antigens in the pancreatic lymph nodes. *J Exp Med* 189: 331–339, 1999.
- Jun HS, Yoon CS, Zbytniuk L, Van Rooijen N, Yoon JW.** The role of macrophages in T cell-mediated autoimmune diabetes in nonobese diabetic mice. *J Exp Med* 189: 347–358, 1999.
- Kawane K, Ohtani M, Miwa K, Kizawa T, Kanbara Y, Yoshioka Y, Yoshikawa H, Nagata S.** Chronic polyarthritis caused by mammalian DNA that escapes from degradation in macrophages. *Nature* 443: 998–1002, 2006.
- Licht R, Jacobs CWM, Tax WJM, Berden JHM.** No constitutive defect in phagocytosis of apoptotic cells by resident peritoneal macrophages from pre-morbid lupus mice. *Lupus* 10: 102–107, 2001.
- Luppi P, Trucco M.** Immunological models of type 1 diabetes. *Horm Res* 52: 1–10, 1999.
- Mahaffy JM, Edelstein-Keshet L.** Modeling cyclic waves of circulating T cells in autoimmune diabetes. *SIAM J Appl Math* 67: 915–937, 2007.
- Marée AFM, Komba M, Dyck C, Łabecki M, Finegood DT, Edelstein-Keshet L.** Quantifying macrophage defects in type 1 diabetes. *J theor Biol* 233: 533–551, 2005.

- Marée AFM, Kublik R, Finegood DT, Edelstein-Keshet L.** Modelling the onset of Type 1 diabetes: can impaired macrophage phagocytosis make the difference between health and disease? *Philos Transact A* 364: 1267–1282, 2006.
- Mathis D, Vence L, Benoist C.**  $\beta$ -Cell death during progression to diabetes. *Nature* 414: 792–798, 2001.
- McIlroy D, Tanaka M, Sakahira H, Fukuyama H, Suzuki M, Yamamura K, Oh-sawa Y, Uchiyama Y, Nagata S.** An auxiliary mode of apoptotic DNA fragmentation provided by phagocytes. *Genes Dev* 14: 549–558, 2000.
- Mendes P.** GEPASI: a software package for modelling the dynamics, steady states and control of biochemical and other systems. *Comput Appl Biosci* 9: 563–571, 1993.
- Mendes P.** Biochemistry by numbers: simulation of biochemical pathways with Gepasi 3. *Trends Biochem Sci* 22: 361–363, 1997.
- Mendes P, Kell DB.** Non-linear optimization of biochemical pathways: applications to metabolic engineering and parameter estimation. *Bioinformatics* 14: 869–883, 1998.
- Motulsky HJ, Christopoulos A.** *Fitting models to biological data using linear and non-linear regression: a practical guide to curve fitting.* San Diego CA: GraphPad Software Inc., 2003.
- O’Brien BA, Fieldus WE, Field CJ, Finegood DT.** Clearance of apoptotic  $\beta$ -cells is reduced in neonatal autoimmune diabetes-prone rats. *Cell Death Differ* 9: 457–464, 2002a.
- O’Brien BA, Geng X, Orteu CH, Huang Y, Ghoreishi M, Zhang Y, Bush JA, Li G, Finegood DT, Dutz JP.** A deficiency in the in vivo clearance of apoptotic cells is a feature of the NOD mouse. *J Autoimmun* 26: 104–115, 2006.
- O’Brien BA, Huang Y, Geng X, Dutz JP, Finegood DT.** Phagocytosis of apoptotic cells by macrophages from NOD mice is reduced. *Diabetes* 51: 2481–2488, 2002b.
- Odaka C, Mizuochi T.** Macrophages are involved in DNA degradation of apoptotic cells in murine thymus after administration of hydrocortisone. *Cell Death Differ* 9: 104–112, 2002.
- Potter PK, Cortes-Hernandez J, Quartier P, Botto M, Walport MJ.** Lupus-prone mice have an abnormal response to thioglycolate and an impaired clearance of apoptotic cells. *J Immunol* 170: 3223–3232, 2003.

- Reefman E, De Jong MCJM, Kuiper H, Jonkman MF, Limburg PC, Kallenberg CGM, Bijl M.** Is disturbed clearance of apoptotic keratinocytes responsible for UVB-induced inflammatory skin lesions in systemic lupus erythematosus? *Arthritis Res Ther* 8: R156, 2006.
- Shimada A, Takei I, Maruyama T, Kasuga A, Kasatani T, Watanabe K, Asaba Y, Ishii T, Tadakuma T, Habu S, et al.** Acceleration of diabetes in young NOD mice with peritoneal macrophages. *Diabetes Res Clin Pract* 24: 69–76, 1994.
- Trudeau JD, Dutz JP, Arany E, Hill DJ, Fieldus WE, Finegood DT.** Neonatal  $\beta$ -cell apoptosis: a trigger for autoimmune diabetes? *Diabetes* 49: 1–7, 2000.
- Trudeau JD, Kelly-Smith C, Verchere CB, Elliott JF, Dutz JP, Finegood DT, Santamaria P, Tan R.** Prediction of spontaneous autoimmune diabetes in NOD mice by quantification of autoreactive T cells in peripheral blood. *J Clin Invest* 111: 217–223, 2003.

## 5 Appendix

### 5.1 Details of formulae

The initial slope of the data curve in the engulfment phase can be approximated by

$$S_1 = \frac{dM_1}{dt} \approx \frac{\text{Change in } M_1}{\text{Elapsed time}} = \frac{M_1(t_1) - M_1(0)}{t_1 - 0} = \frac{M_1(t_1)}{t_1}. \quad (3)$$

A similar result holds for  $S_0$ , the magnitude of slope of the curve  $M_0$ .

In the digestion phase (assuming parallel digestion), the change in the phagocytic index,  $I_\Phi$ , satisfies a simple linear first-order differential equation whose solution is

$$I_\Phi(t) = \tilde{I}_\Phi e^{-k_d T}, \quad (4)$$

where  $\tilde{I}_\Phi$  is the phagocytic index at the start of the digestion phase, and  $T = t - t_{d0}$ . Rearrangement of this formula leads to Eq. (2).

### 5.2 Akaike weights

The Akaike's Information Criterion ( $AIC$ ) (Akaike, 1973; Motulsky and Christopoulos, 2003) maximizes the probability that a candidate model generated the observed data by rewarding descriptive accuracy, while penalizing an increase in the number of free parameters. We have used the corrected version,

$$AIC_c = n \ln \left( \frac{SSE}{n} \right) + 2K + \frac{2K(K+1)}{n-K-1}, \quad (5)$$

where  $n$  is the number of observations,  $K$  the number of fitted parameters, and  $SSE$  the remaining sum of squared error after curve-fitting. The model with lowest  $AIC_c$  value is considered to be the best model with most parsimonious description of the data. The Akaike weight,  $w_i$  represents the probability that model  $i$  is the best model, given the data and the set of candidate models:

$$w_i = \frac{e^{-0.5 \cdot \Delta_i(AIC_c)}}{\sum_{j=1}^M e^{-0.5 \cdot \Delta_j(AIC_c)}}, \quad (6)$$

where  $M$  is the total number of models, the minimum is taken over all candidate models, and where  $\Delta_i(AIC_c) = (AIC_c)_i - \min(AIC_c)$ . Relative probabilities of any two models are proportional to the weights computed for them, regardless of the total number of models being compared. The advantage of the  $AIC$  method is that it allows us to compare all of the models simultaneously as easily as a subset of these models.

## 6 Tables and Figures

Table 1: **Measured quantities used in ballpark estimates of parameters.** For good estimates it is important to have measurements of the number of macrophages  $M_0(t)$ ,  $M_1(t)$  at an early time point  $t_1 = 20$  min (shortly after the feeding experiment is started). All classes should be quantified at intermediate times  $t_Q$  (at 1, 2h). At these times, the ratio of macrophages in successive classes ( $M_{i+1}/M_i$ ) is roughly constant. Finally, apoptotic cells are washed out at  $t = 2$ h and further measurements are made during the *digestion phase*, at  $t_d = 2, 3, 4, 5$  h, when no more engulfments are taking place. This helps to get independent estimates of the digestion rate.

quantity	symbol	measurement times
<b>Total number of macrophages</b>	$M$	$t = 0$
<b>Initial number of apoptotic cells</b>	$A$	$t = 0$
<b>Number of macrophages with</b>		
0 visible engulfed apoptotic cells	$M_0(t)$	$t = t_1, t_Q; t_d$
1 visible engulfed apoptotic cells	$M_1(t)$	$t = t_1, t_Q; t_d$
2 visible engulfed apoptotic cells	$M_2(t)$	$t = t_1, t_Q; t_d$
$\vdots$	$\vdots$	$\vdots$
n visible engulfed apoptotic cells	$M_n(t)$	$t = t_Q; t_d$

Table 2: **A list of calculated values that lead to ballpark estimates of the rates of engulfment, activation, and digestion, with the time points on which they are based.**  $t_1$  is an early time point close to the beginning of the feeding,  $t_Q$  is intermediate, and  $t_d$  represents (multiple) time points in the digestion phase of the experiment, after the apoptotic cells are washed out. Detailed derivations of these formulae are given in Marée et al. (2005).

Symbol	Meaning	Calculation	Time	Formula
<b>Generic calculated values</b>				
$R$	ratio of macrophages in successive classes	$= M_{i+1}/M_i$	$t_Q$	[r1]
$S_0$	slope of initial engulfment	$= (M - M_0)/t_1$	$t_1$	[s0]
$S_1$	slope of initial rise of $M_1$	$= M_1/t_1$	$t_1$	[s1]
$S_2$	slope of initial rise of $M_2$	$= M_2/t_1$	$t_1$	[s2]
$\Phi$	percent phagocytosis	$= (100/M) \cdot \sum_{i=1}^n M_i$	any	[p1]
$I_\Phi$	phagocytic index	$= (100/M) \cdot \sum_{i=1}^n (i M_i)$	any	[i1]
<b>Parameters in Basic Model</b>				
$R$	ratio of macrophages in successive classes	$= k_e A/k_d$	$t_Q$	[r2]
		$= \Phi/100$	$t_Q$	[r3]
		$= I_\Phi/(100 + I_\Phi)$	$t_Q$	[r4]
$k_e$	rate of engulfment	$= S_1/MA$	$t_1$	[e1]
		$= S_0/MA$	$t_1$	[e2]
$k_d$	rate of digestion (serial)	$= k_e A/R$	$t_Q$	[d1]
		$= \frac{k_e AM}{M - M_0}$	$t_Q$	[d2]
		$= k_e A \left( \frac{100}{I_\Phi} + 1 \right)$	$t_Q$	[d3]
<b>Parameters in model with activation</b>				
$R_a$	ratio of macrophages in classes 0 and 1	$= M_1/M_0$	$t_Q$	[r5]
$R$	ratio of macrophages in successive classes	$= M_{i+1}/M_i, i \geq 1$	$t_Q$	[r6]
$k_a$	rate of activation	$= S_0/MA$	$t_1$	[a1]
$k_e$	rate of engulfment	$= S_2/M_1A$	$t_1$	[e3]
		$= k_a R/R_a$	$t_Q$	[e4]
		$= \frac{k_a}{\Phi^2} (I_\Phi - \Phi)(100 - \Phi)$	$t_Q$	[e5]
<b>Parameters in unsaturated digestion model</b>				
$k'_d$	rate of digestion (parallel)	$= \frac{1}{t - t_{d0}} \ln \left( \frac{I_\Phi(t_{d0})}{I_\Phi(t)} \right)$	$t_d$	[d4]

Table 3: **Rough estimates of the kinetic parameters for engulfment and digestion of apoptotic cells by macrophages.** We used the formulae in Table 2 to estimate these quantities. For estimates at  $t_Q$ , (at QSS) the time points at 1 and 2 hours are used. The values are given as mean  $\pm$  SD. In the last column, we show the 95% confidence interval for the computed fold difference (i.e. ratio of BALB/c to NOD parameter value). Asterisks indicate  $P < 0.05$ .

parameter	based on Eq.	# measurements	BALB/c	NOD	fold diff.
<b>Basic Model</b>					
$k_e$ ( $10^{-7}$ mL cell $^{-1}$ h $^{-1}$ )	[e1]	5	$4.28 \pm 1.85$	$1.65 \pm 0.85$	$2.59 \pm 1.27^*$
$k_e$ ( $10^{-7}$ mL cell $^{-1}$ h $^{-1}$ )	[e2]	5	$5.87 \pm 3.32$	$1.80 \pm 0.92$	$3.25 \pm 1.97^*$
$k_d$ (h $^{-1}$ )	[d1]	70	$1.20 \pm 1.55$	$0.94 \pm 1.36$	$1.27 \pm 0.52$
$k_d$ (h $^{-1}$ )	[d2]	10	$1.38 \pm 0.69$	$1.27 \pm 1.09$	$1.09 \pm 0.67$
$k_d$ (h $^{-1}$ )	[d3]	10	$1.25 \pm 0.69$	$1.26 \pm 1.08$	$0.99 \pm 0.67$
<b>model variant I</b>					
$k_a$ ( $10^{-7}$ mL cell $^{-1}$ h $^{-1}$ )	[a1]	5	$5.87 \pm 3.32$	$1.80 \pm 0.92$	$3.25 \pm 1.97^*$
$k_e$ ( $10^{-7}$ mL cell $^{-1}$ h $^{-1}$ )	[e4]	10	$15.9 \pm 18.9$	$1.84 \pm 1.44$	$8.64 \pm 6.85^*$
$k_e$ ( $10^{-7}$ mL cell $^{-1}$ h $^{-1}$ )	[e5]	10	$10.5 \pm 8.2$	$1.91 \pm 0.48$	$5.49 \pm 2.84^*$
<b>model variant III</b>					
$k'_d$ (h $^{-1}$ apopt. body $^{-1}$ )	[d4]	120	$0.30 \pm 0.094$	$0.28 \pm 0.079$	$1.09 \pm 0.08^*$

Table 4: **Best fits for the kinetic parameters describing engulfment, activation and digestion of apoptotic cells by macrophages for the various models.** The values are given as mean  $\pm$  SD. In the last column, we show the 95% confidence interval for the computed fold difference (i.e. ratio of BALB/c to NOD parameter value). Asterisks indicate  $P < 0.05$ . Each parameter estimate is based on concurrent data fitting to 30 measurements using the full data set and the optimization feature of the software Gepasi.

parameter	BALB/c	NOD	fold diff.
<b>Full dataset</b>			
<b>Basic Model</b>			
$k_e$ ( $10^{-7}$ mL cell $^{-1}$ h $^{-1}$ )	8.14 $\pm$ 0.342	2.38 $\pm$ 0.008	3.42 $\pm$ 0.05*
$k_d$ (h $^{-1}$ )	0.608 $\pm$ 0.0291	0.348 $\pm$ 0.0019	1.75 $\pm$ 0.03*
SD of full model	10734.4	582.2	
<b>model variant I (reversible activation)</b>			
$k_a$ ( $10^{-7}$ mL cell $^{-1}$ h $^{-1}$ )	5.45 $\pm$ 0.206	2.1 $\pm$ 0.007	2.59 $\pm$ 0.04*
$k_e$ ( $10^{-7}$ mL cell $^{-1}$ h $^{-1}$ )	21.6 $\pm$ 1.23	4.05 $\pm$ 0.036	5.34 $\pm$ 0.11*
$k_d$ (h $^{-1}$ )	0.615 $\pm$ 0.0388	0.312 $\pm$ 0.0021	1.97 $\pm$ 0.05*
SD of full model	7995.9	537.3	
<b>model variant II (irreversible activation) (<math>N = 7</math>)</b>			
$k_a$ ( $10^{-7}$ mL cell $^{-1}$ h $^{-1}$ )	5.39 $\pm$ 0.175	2.08 $\pm$ 0.007	2.59 $\pm$ 0.03*
$k_e$ ( $10^{-7}$ mL cell $^{-1}$ h $^{-1}$ )	23.6 $\pm$ 1.42	4.25 $\pm$ 0.039	5.54 $\pm$ 0.12*
$k_d$ (h $^{-1}$ )	0.782 $\pm$ 0.0436	0.324 $\pm$ 0.0022	2.41 $\pm$ 0.05*
SD of full model	7920.2	535.8	
<b>model variant II (irreversible activation) (<math>N = 12</math>)</b>			
$k_a$ ( $10^{-7}$ mL cell $^{-1}$ h $^{-1}$ )	5.40 $\pm$ 0.177	2.08 $\pm$ 0.007	2.59 $\pm$ 0.03*
$k_e$ ( $10^{-7}$ mL cell $^{-1}$ h $^{-1}$ )	23.6 $\pm$ 1.47	4.26 $\pm$ 0.039	5.55 $\pm$ 0.13*
$k_d$ (h $^{-1}$ )	0.782 $\pm$ 0.0442	0.325 $\pm$ 0.0022	2.41 $\pm$ 0.05*
SD of full model	7974.4	535.8	
<b>model variant III (parallel digestion)</b>			
$k_a$ ( $10^{-7}$ mL cell $^{-1}$ h $^{-1}$ )	3.83 $\pm$ 0.115	1.91 $\pm$ 0.006	2.01 $\pm$ 0.02*
$k_e$ ( $10^{-7}$ mL cell $^{-1}$ h $^{-1}$ )	25.6 $\pm$ 2.05	5.57 $\pm$ 0.061	4.59 $\pm$ 0.14*
$k'_d$ (h $^{-1}$ apopt. body $^{-1}$ )	0.313 $\pm$ 0.0243	0.292 $\pm$ 0.0021	1.07 $\pm$ 0.03*
SD of full model	8544.8	542.7	
<b>model variant IV (saturated digestion)</b>			
$k_a$ ( $10^{-7}$ mL cell $^{-1}$ h $^{-1}$ )	5.10 $\pm$ 0.163	2.01 $\pm$ 0.007	2.54 $\pm$ 0.03*
$k_e$ ( $10^{-7}$ mL cell $^{-1}$ h $^{-1}$ )	24.9 $\pm$ 1.94	4.72 $\pm$ 0.071	5.28 $\pm$ 0.15*
$k_d$ (h $^{-1}$ )	1.08 $\pm$ 0.199	0.626 $\pm$ 0.0400	1.72 $\pm$ 0.12*
$c$ (apopt. bodies)	0.713 $\pm$ 0.340	1.00 $\pm$ 0.125	0.71 $\pm$ 0.13*
SD of full model	7952.6	541.0	
<b>Digestion phase only</b>			
<b>model variant I (serial digestion)</b>			
$k_d$ (h $^{-1}$ )	0.739 $\pm$ 0.0297	0.35 $\pm$ 0.0016	2.11 $\pm$ 0.04*
SD of full model	7721.7	498.2	
<b>model variant III (parallel digestion)</b>			
$k'_d$ (h $^{-1}$ apopt. body $^{-1}$ )	0.409 $\pm$ 0.0167	0.301 $\pm$ 0.0014	1.36 $\pm$ 0.03*
SD of full model	8739.3	523.4	
<b>model variant IV (saturated digestion)</b>			
$k_d$ (h $^{-1}$ )	1.29 $\pm$ 0.223	0.569 $\pm$ 0.0286	2.27 $\pm$ 0.21*
$c$ (apopt. bodies)	1.19 $\pm$ 0.423	0.686 $\pm$ 0.0847	1.73 $\pm$ 0.33*
SD of full model	7609.18	512.211	



Table 5: **Model comparisons using the corrected Akaike's Information Criterion  $AIC_c$  (Eqs. (5)-(6)).**  $n$  = number of observations;  $K$  = number of fitted parameters. Models that are most probable have lowest values of  $AIC_c$  and highest  $w_i$ . (Absolute  $AIC_c$  values are not significant, but relative  $w_i$  values directly indicate the relative probabilities of the models.) Model variants I, II: reversible, irreversible activation; variants III, IV: parallel, saturated digestion. It is very unlikely that replicates truly vary in their kinetic parameters, because replicate fits systematically lead to very low relative values of the weights  $w_i$ .

data	Fitting	Model	Strain	$SSE$	$n$	$K$	$AIC_c$	$w_i$
all	replicate	Basic Model	BALB/c	$3.20 \cdot 10^9$	10	30	586.15	0.00 %
all	replicate	variant I	BALB/c	$9.48 \cdot 10^8$	15	30	582.36	0.00 %
all	replicate	variant II ( $N = 7$ )	BALB/c	$9.34 \cdot 10^8$	15	30	581.90	0.00 %
all	replicate	variant II ( $N = 12$ )	BALB/c	$9.55 \cdot 10^8$	15	30	582.57	0.00 %
all	replicate	variant III	BALB/c	$1.32 \cdot 10^9$	15	30	592.34	0.00 %
all	replicate	variant IV	BALB/c	$9.18 \cdot 10^8$	20	30	650.42	0.00 %
all	concurrent	Basic Model	BALB/c	$3.23 \cdot 10^9$	2	30	559.25	0.01 %
all	concurrent	variant I	BALB/c	$1.73 \cdot 10^9$	3	30	542.96	24.42 %
all	concurrent	variant II ( $N = 7$ )	BALB/c	$1.69 \cdot 10^9$	3	30	542.39	32.48 %
all	concurrent	variant II ( $N = 12$ )	BALB/c	$1.72 \cdot 10^9$	3	30	542.80	26.48 %
all	concurrent	variant III	BALB/c	$1.97 \cdot 10^9$	3	30	546.95	3.33 %
all	concurrent	variant IV	BALB/c	$1.64 \cdot 10^9$	4	30	544.18	13.28 %
all	replicate	Basic Model	NOD	$1.64 \cdot 10^7$	10	30	427.98	0.00 %
all	replicate	variant I	NOD	$1.28 \cdot 10^7$	15	30	453.09	0.00 %
all	replicate	variant II ( $N = 7$ )	NOD	$1.27 \cdot 10^7$	15	30	453.06	0.00 %
all	replicate	variant II ( $N = 12$ )	NOD	$1.27 \cdot 10^7$	15	30	453.06	0.00 %
all	replicate	variant III	NOD	$1.25 \cdot 10^7$	15	30	452.41	0.00 %
all	replicate	variant IV	NOD	$1.18 \cdot 10^7$	20	30	519.68	0.00 %
all	concurrent	Basic Model	NOD	$9.49 \cdot 10^6$	2	30	384.38	4.04 %
all	concurrent	variant I	NOD	$7.80 \cdot 10^6$	3	30	380.96	22.34 %
all	concurrent	variant II ( $N = 7$ )	NOD	$7.75 \cdot 10^6$	3	30	380.79	24.31 %
all	concurrent	variant II ( $N = 12$ )	NOD	$7.75 \cdot 10^6$	3	30	380.79	24.30 %
all	concurrent	variant III	NOD	$7.95 \cdot 10^6$	3	30	381.55	16.59 %
all	concurrent	variant IV	NOD	$7.61 \cdot 10^6$	4	30	382.91	8.43 %
digestion only	replicate	Basic Model	BALB/c	$5.34 \cdot 10^8$	5	15	277.48	1.25 %
digestion only	replicate	variant III	BALB/c	$1.07 \cdot 10^9$	5	15	287.97	0.01 %
digestion only	replicate	variant IV	BALB/c	$4.86 \cdot 10^8$	10	15	334.39	0.00 %
digestion only	concurrent	Basic Model	BALB/c	$8.35 \cdot 10^8$	1	15	269.83	57.35 %
digestion only	concurrent	variant III	BALB/c	$1.07 \cdot 10^9$	1	15	273.54	8.96 %
digestion only	concurrent	variant IV	BALB/c	$7.53 \cdot 10^8$	2	15	270.97	32.43 %
digestion only	replicate	Basic Model	NOD	$6.50 \cdot 10^6$	5	15	211.35	0.00 %
digestion only	replicate	variant III	NOD	$6.13 \cdot 10^6$	5	15	210.47	0.00 %
digestion only	replicate	variant IV	NOD	$4.98 \cdot 10^6$	10	15	265.69	0.00 %
digestion only	concurrent	Basic Model	NOD	$3.48 \cdot 10^6$	1	15	187.60	56.29 %
digestion only	concurrent	variant III	NOD	$3.84 \cdot 10^6$	1	15	189.09	26.85 %
digestion only	concurrent	variant IV	NOD	$3.41 \cdot 10^6$	2	15	190.02	16.86 %

Table 6: **Summary of experimental observations and results of experimental refinements from modeling efforts.**

<b>Citation</b>	<b>Experiments done</b> (time points observed)	<b>Issues with parameter identification</b>
O'Brien et al. (2002b) (older work)	intermediate times	poor resolution of $k_a$ (and hence of all other parameters)
Marée et al. (2005) (previous paper)	early and intermediate times	$k_a$ well characterized; poor resolution of $k_d$ because $A$ cannot be measured (and hence poor resolution of $k_e$ as well)
this paper	early and intermediate times as well as decay phase	independent estimates of $k_a$ , $k_e$ and $k_d$ ; all parameters well characterized

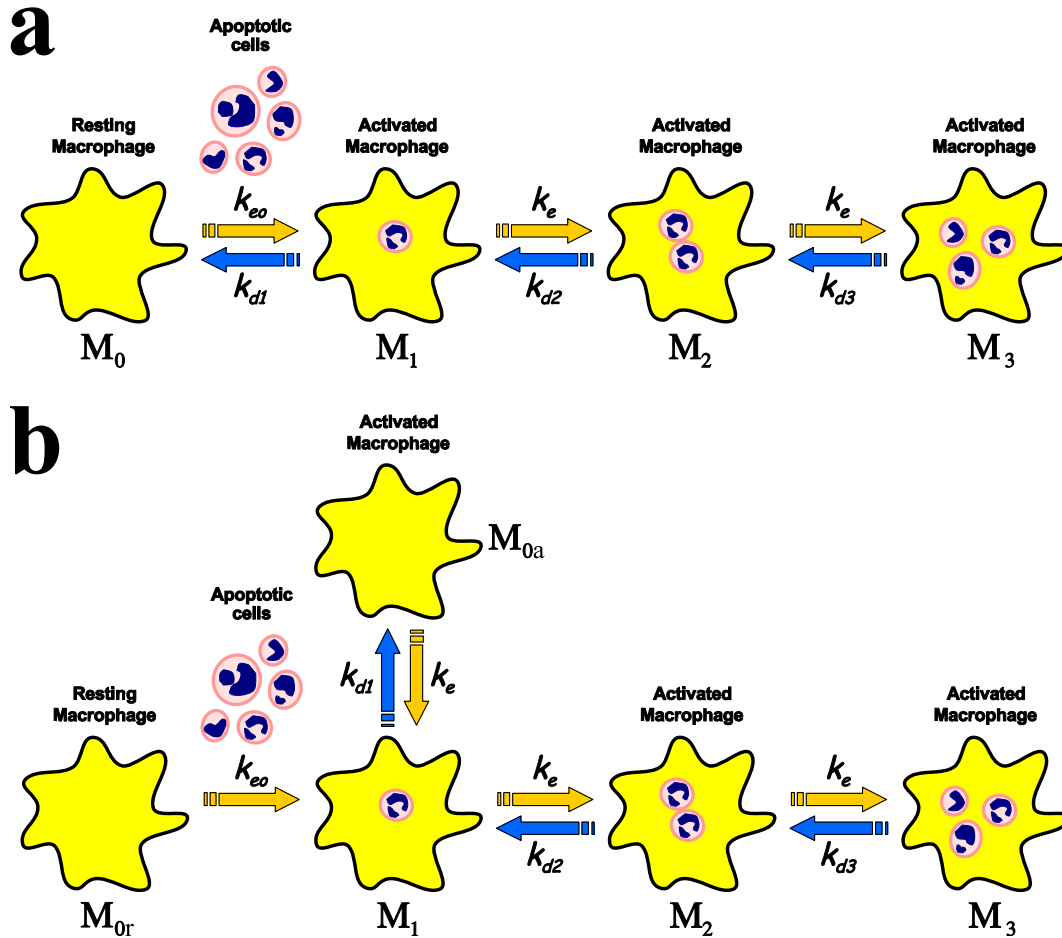


Figure 1: A schematic illustrating the models used here to analyze macrophage dynamics. (a) The Basic Model and variant I with reversible activation; (b) Variant II–IV, with irreversible activation. The arrows represent uptake of apoptotic cells by phagocytosis (yellow arrows pointing right or down), and digestion of those apoptotic bodies (blue arrows pointing left or up).  $M_n$  represents the class of macrophages that contain  $n$  visible engulfed apoptotic bodies. (For example,  $M_0$  is the class of macrophages that have no visible apoptotic bodies inside them, and include macrophages that have not yet engulfed or those that have already digested all their internalized apoptotic cells.)  $k_a$  represents the rate of initial engulfment (and the “activation” rate),  $k_e$  represents the subsequent engulfment rate, and  $k_d$  is the rate of digestion. Model variants considered were: Basic Model: all digestion rates identical ( $k_{d1} = k_{d2} = k_{d3} = k_d$ ), all engulfment rates identical ( $k_{eo} = k_e$ ), and no activation step. Variant I: Reversible activation: as in Basic model, but with  $k_{eo} = k_a \neq k_e$ . Variant II: Irreversible activation: as in Variant I, but including activated macrophages without visible apoptotic bodies inside them. We considered two versions of this variant, with maximal macrophage capacity of  $N = 7$  and  $N = 12$ . Variant III: Parallel digestion: as in Variant II, but with  $k_{d1} = k'_d, k_{d2} = 2k'_d, k_{d3} = 3k'_d$ , etc. Variant IV: Saturated digestion: as in Variant II, but with  $k_{d1} = k_d/(c + 1), k_{d2} = 2k_d/(c + 2), k_{d3} = 3k_d/(c + 3)$ , etc. Some elements of figure credited to C. Dyke.

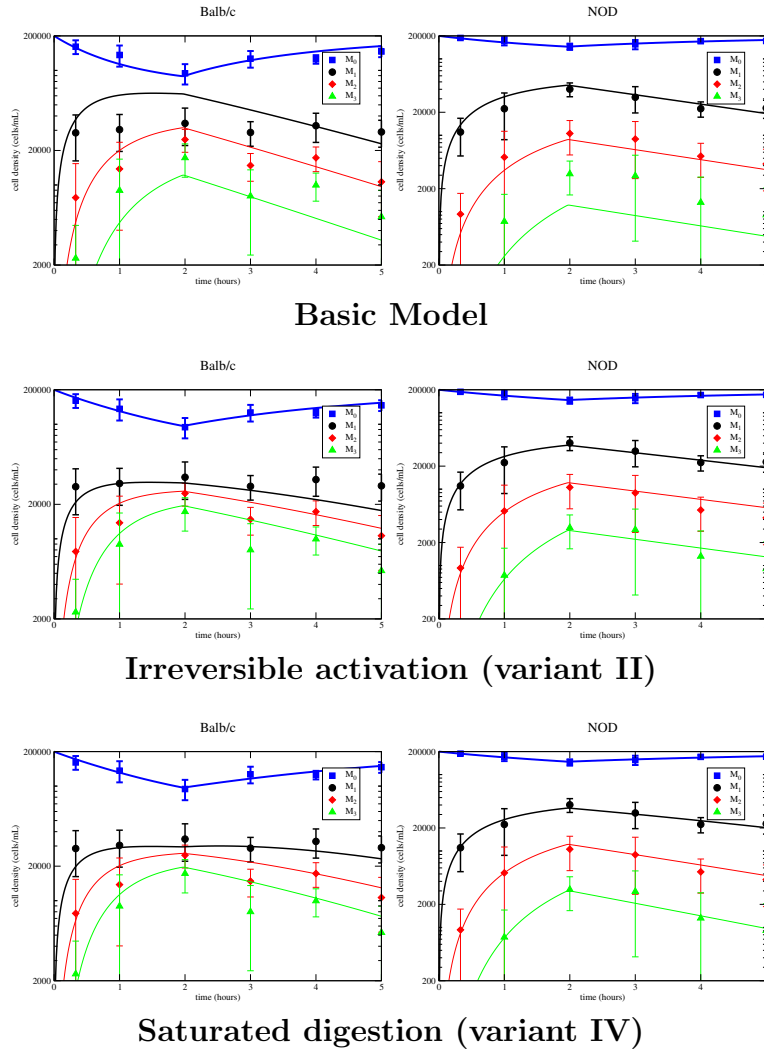


Figure 2: A comparison of three models, showing BALB/c macrophage phagocytosis data (left column) and NOD data (right column) over the 5 hour experiment. Each curve represents the number of macrophages in a given class, with none ( $M_0$ , shown in blue), or with 1, 2, or 3 visible internalized apoptotic bodies. At  $t = 2$  h, the residual unengulfed apoptotic cells were washed out. The period  $2 \text{ h} < t < 5 \text{ h}$  is the “digestion-only phase”, in which digestion is the only process occurring. We found that a model with an activation step, variant II (or I, not shown) fits the BALB/c data significantly better than the Basic Model. Saturated digestion (variant IV) fits the data best, but uses one more parameter, making it a less parsimonious description of the dynamics.

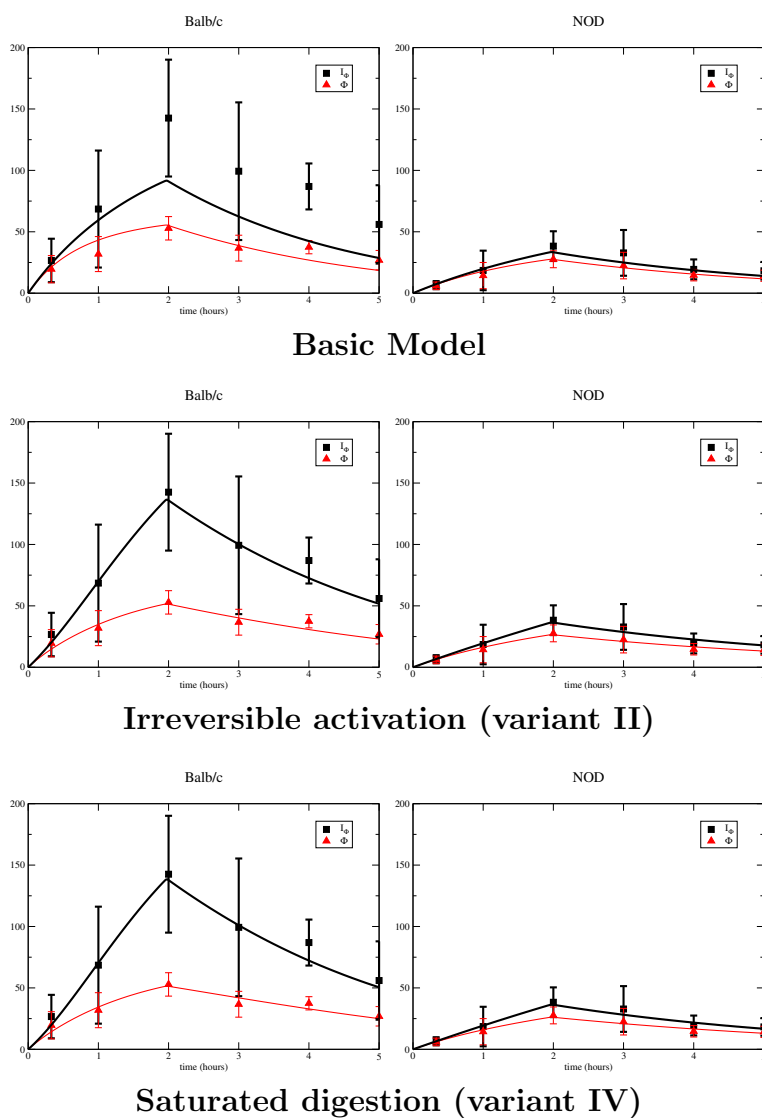


Figure 3: Fits of the data to models shown in Figure 2 resulted in these predictions of the percent phagocytosis  $\Phi$  and the phagocytic index  $I_\Phi$  over the course of the 5-hour experiment.